Investigations of stratospheric temperature regional variability with lidar and Advanced Microwave Sounding Unit

Beatriz M. Funatsu, Chantal Claud, Philippe Keckhut, Wolfgang Steinbrecht, Alain Hauchecorne

Investigations of stratospheric temperature regional variability with lidar and Advanced Microwave Sounding Unit

Beatriz M. Funatsu,[1,2] Chantal Claud,[2] Philippe Keckhut,[1] Wolfgang Steinbrecht,[3] and Alain Hauchecorne[1]

Received 9 August 2010; revised 1 February 2011; accepted 3 February 2011; published 19 April 2011.

[1] Seasonal and interannual stratospheric temperature variability at two relatively close-by lidar stations, the Observatoire de Haute-Provence (France) and the Hohenpeissenberg Observatory (Germany), are investigated using lidars and the Advanced Microwave Sounding Unit (AMSU) satellite data to examine possible causes of temperature trend discrepancies between these two sites. We first examined data measured by lidar and AMSU at each station and found that temperature anomalies observed with lidar have larger spread than those with AMSU probably as a result of distinct vertical sampling. Lidar and AMSU measurements have correlation typically higher than 0.7; however, correlation is decreased to 0.4–0.5 in summer at the French station. Lidar measurements have good correlation between the two stations, around 0.9 in winter and 0.45 in summer, while AMSU data show correlations between both stations of about 0.94 year-round. Data from coincident measurement dates at both sites have then been taken from the integral series in order to isolate local geophysical effects. A comparison between lidar and AMSU measurements of coincident dates suggests that in wintertime measurement discrepancies are to a great extent a result of different local atmospheric dynamics. These are important on the estimation of stratospheric trends and can partially explain discrepancies observed in trends estimates based on lidars in distinct locations or on satellite data. The present results have implications on the planning of measurement strategies using lidars involved in the Network for the Detection of Atmospheric Composition Changes (NDACC), as well as on methodologies for satellite data use for stratospheric monitoring purposes.

Citation: Funatsu, B. M., C. Claud, P. Keckhut, W. Steinbrecht, and A. Hauchecorne (2011), Investigations of stratospheric temperature regional variability with lidar and Advanced Microwave Sounding Unit, *J. Geophys. Res.*, *116*, D08106, doi:10.1029/2010JD014974.

1. Introduction

[2] Over the period 1979–2005 the stratosphere has cooled significantly [*Ramaswamy et al.*, 2001] for a number of reasons: stratospheric ozone depletion, increase of well-mixed greenhouse gases and water vapor, dynamical changes [e.g., *Shine et al.*, 2003; *Cagnazzo et al.*, 2006; *Austin et al.*, 2009]. Confidence in the magnitude of the observed trends is higher for the lower stratosphere [*Randel et al.*, 2009], where longer data records and better homogeneity adjustments are available. In the middle and upper stratosphere; however, there is a need for an improved understanding of the reliability of the underlying data. Apart from the now defunct rocket network [e.g., *Ramaswamy et al.*, 2001] satellites and ground-based lidars are currently the only sources of long-term data for monitoring middle and upper stratospheric temperature.

[3] Between 1979 and 2005 the only near-global source of temperatures in the middle atmosphere on a long-term basis were the successive Stratospheric Sounding Unit (SSU) instruments put into orbit onboard the National Oceanic and Atmospheric Administration (NOAA) TIROS-N satellites. As reviewed, e.g., by *Randel et al.* [2009], the production of a consistent record over more than two decades from these operational data presents many challenges, mainly because it relies on several satellites whose orbit can drift with time [*Gelman et al.*, 1986; *Nash and Forrester*, 1986] and sometimes differ by 12 h [*Keckhut et al.*, 2001]. The problem is further complicated by the fact that measurements are made in the 15 μm band of CO_2, and that weighting functions have shifted to higher altitudes as the amount of CO_2 in the atmosphere increased [*Shine et al.*, 2008]. The only other continuous and ongoing observation of temperature in the middle and upper stratosphere is from lidar nighttime measurements. Long-term records are available in the frame of the Network for the Detection of Atmospheric Composition Change (NDACC), formerly the Network for the Detection of Stratospheric Change (NDSC) [*Kurylo and Solomon*, 1990].

[1] Laboratoire Atmosphères, Milieux, Observations Spatiales, Université Versailles-Saint Quentin, Guyancourt, France.
[2] Laboratoire de Meteorologie Dynamique, Ecole Polytechnique, Palaiseau, France.
[3] Meteorologisches Observatorium, Hohenpeissenberg, Germany.

0148-0227/11/2010JD014974

Several stations provide decadal and homogeneous series [*Keckhut et al.*, 2004]. *Randel et al.* [2009] noted that comparing trends obtained by SSU and by lidars is difficult because of the very different sampling: Localized lidar observations versus zonal mean SSU, and limited temporal sampling of the lidars (clear nights only) versus true monthly mean of SSU. Consequently, temperature anomalies recorded by lidars located in the midlatitudes show much more variability in their time series than that captured by SSU. *Keckhut et al.* [2011] have further analyzed differences between lidar and satellites over the period 1979–2005 and concluded that changes in the satellite weighting functions cannot explain all the differences. Both studies point out that lidar and satellite derived trends have discrepancies that are not fully understood. This is true even for trends derived from lidar measurements from two relatively close-by stations, the Observatoire de Haute Provence (OHP, 43.8°N, 5.7°E) in France and the Hohenpeissenberg Observatory (HOH, 47.8°N, 11.0°E) in Germany, which exhibit significant differences not only in temperature [e.g., *Randel et al.*, 2004, 2009] but in stratospheric ozone trends as well [*Steinbrecht et al.*, 2006]. For example, OHP temperature records between 1988 and 2005 show cooling weaker than −1.0 K/decade in the layer between 40 and 55 km, while HOH present warming of 0.5–1.0 K/decade for the same period and altitudes [see, e.g., *Randel et al.*, 2009, Figure 22]. Moreover, *Steinbrecht et al.* [2006] showed that for the period 1997–2005 OHP ozone series averaged over a layer of 35 to 45 km of altitude presented a positive trend of around +1%/decade (suggesting that ozone begins to recover in the upper stratosphere), while at HOH the trend is negative, around −2.5%/decade. These differences in trends estimates emerge because of a combination of (1) temporal sampling, (2) instrument differences, and/or (3) the different geographical location. Issue 1 arises from the fact that lidars temperature measurements are made only in nights without visible clouds (therefore discontinuous) and vary from one station to another because of local weather conditions. Temporal sampling can lead to differences in monthly mean temperature calculation, and subsequently on temperature trend estimation [*Funatsu et al.*, 2008].

[4] In this work, we seek to further investigate the causes of temperature trend discrepancies between OHP and HOH, by using another independent data source. We choose the Advanced Microwave Sounding Unit (AMSU) satellite data, which have replaced the SSU [*Ho et al.*, 2007; *Steiner et al.*, 2007; *Mo*, 2009, 2010]. Compared to its predecessor, AMSU has an improved vertical and horizontal resolution, and in addition, raw data are publicly available for all orbits, unlike the SSU for which we had for the long-term calibrated series only 10° latitude zonal means. The strategy applied was to compare lidar and AMSU satellite data based only on those nights when there were measurements at both lidar stations. Because AMSU-derived temperature series for each station are based on the same instrument, it should become possible to separate differences arising from the use of different lidar instruments at OHP and HOH, from differences resulting from the different geographical location of the two lidar stations.

[5] The paper is structured as follows: The data are briefly presented in section 2, followed by an analysis of lidar and AMSU measurements in terms of annual cycle and temperature anomalies in section 3. We then focus on the discrepancies found between AMSU and lidar-derived data using only coincident dates of lidars measurements (section 4). Summary and results are presented in the last section 5.

2. Data

[6] The Observatoire de Haute Provence is located in southern France and has the longest lidar temperature series, starting in 1979 [*Hauchecorne and Chanin*, 1980; *Keckhut et al.*, 1993]. Temperature profiles are derived from molecular scattering caused by the emission of a short-duration laser pulse in the zenith direction. The typical integration time is 2 to 4 h. The Hohenpeissenberg Observatory in Germany, located at around 600 km northeast of OHP, collects measurements of ozone and temperature since 1987 with a Differential Absorption Lidar system. Instrument description and setup can be found in the work of *Steinbrecht et al.* [2009a]. A comprehensive comparison between the instruments is given by *Keckhut et al.* [2004].

[7] Measurement uncertainties at OHP for the period 1998–2005 are usually below 1 K at 50 km except for short periods in 1996, 1998, and 2001 because of adjustments of lidar instrument [*Keckhut et al.*, 2004, 2011]. Uncertainties at the same altitude at HOH are larger, around 2 to 4 K on average [*Steinbrecht et al.*, 2009a; *Keckhut et al.*, 2011]. At lower altitudes, around 40 km, the uncertainties are much smaller, of the order of 0.3 K or less at OHP and ranging from 1.0 to 3.0 K at HOH. These are the altitudes we are interested in for the present study. For both sites we perform a 3 km running mean for each temperature profile [*Funatsu et al.*, 2008].

[8] The Advanced Microwave Sounding Unit is an atmospheric vertical sounder flying onboard polar orbiting American (NOAA-15 through 19) and European (MetOp-A) satellites. The first AMSU instrument was launched onboard NOAA-15 in late 1998. It is currently the sentinel satellite for stratospheric temperature monitoring and will hopefully insure continuity for at least one more decade. In the present study we use data from NOAA-16 only in order to avoid intersatellite biases. Also, only night passes (that is, between 2200 and 0500 UTC) are considered, as lidar measurements are done at night. AMSU is composed of two modules sounding the atmosphere in the microwave frequency domain, with 20 channels in total. Here we are interested in module A which provides near-surface and atmospheric (until the upper stratosphere) temperature information. Details on instrument, channels and weighting functions can be found in the work of, e.g., *Goldberg et al.* [2001]. We focus on channels 12 to 14 which have weighting functions peaking between ~30–45 km (Figure 1) and thus provide temperature data above 25 km. These channels have wide weighting functions with a full width at half maximum of ~10 km. The noise level of AMSU-A is expect to be 0.40, 0.54 and 0.91 K for channels 12, 13 and 14, respectively [*Goldberg et al.*, 2001], but were estimated to be slightly smaller (0.35, 0.49 and 0.81 K, respectively) for NOAA-16 by *Wu* [2004].

[9] We derive and use a daily "time series" of AMSU brightness temperatures (BTs) for two target regions: [40°–45°N] [10°W–20E] and [45°–50°N][10°W–20°E]. We use data from 2001 to 2008, covering several annual cycles for both lidar and AMSU. The first overpass region includes

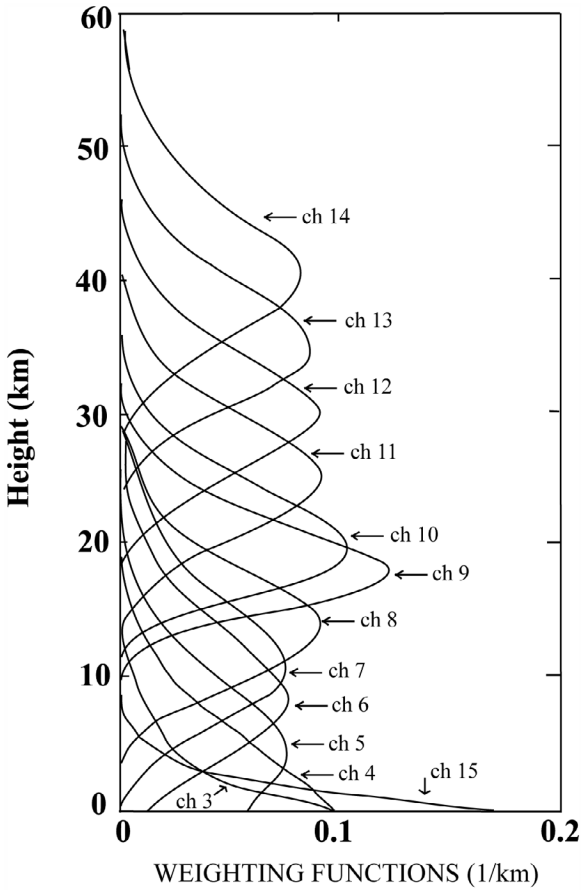

Figure 1. Advanced Microwave Sounding Unit (AMSU)-A weighting functions for channels 3 to 15, for a U.S. standard tropical atmosphere at nadir (from the work of *Karbou et al.* [2005]).

OHP, the latter HOH; hereafter we refer to these series as AMSU@OHP and AMSU@HOH. Because of limb-effect issues that affect temperatures for large viewing angles, only BTs from the field of view closest to nadir (15 and 16) are used in the averaging process, as was done by *Funatsu et al.* [2008]. Correction coefficients for limb effect are time and space dependent, and add to the measurement error. Although the target region is relatively broad in longitude we use only a narrow strip within this area corresponding to the near-nadir measurements to calculate the average nightly BT (the added cross-track distance for the two near-nadir fields of view is of only ~100 km). Notice, however, that the effective target area can be anywhere within the 30° longitude window. Narrowing the target area longitude range to 10° would cause a reduction of about 50% on the number of overpasses falling within the target area, shrinking considerably the sample population.

[10] Figure 2a shows the number of dates per month and year with lidar measurement at OHP and HOH, and Figure 2b shows the total coincident measurement dates per month in this period. Except for a few months, OHP usually presents more measurements per month than HOH. During the period 2001–2008 only on 263 nights both sites had measurements on the same night. *Funatsu et al.* [2008] showed that AMSU-derived monthly mean BT anomalies for a region around OHP have high correlation with monthly mean temperature anomalies measured by the lidar (between 0.76 to 0.9 depending on the height/channel), when using only same dates of lidar measurements to form the monthly means. They found that when using all available night passes of AMSU to form monthly means the correlation with lidar-based measurements decreased to around 0.6–0.8. Furthermore, temporal sampling was shown to have an important impact on the estimation of temperature tendencies. In the present study, AMSU@OHP and AMSU@HOH daily time series were constructed based on nights were lidar measurements were taken at each site.

[11] The temperature (T) time series for HOH and OHP at 32 km are presented in Figure 3, while Figure 4 shows a six-month average of vertical profiles for "summer" (April through September) and "winter" (October through March). Two seasons are considered as planetary waves propagate during winter (generating stratospheric warmings) leading to distinct seasonal temperature variability. Both Figures 3 and 4 point to consistent T differences between the two sites, with colder/warmer T in winter/summer at HOH at most levels up to 45 km. The standard deviation is of the same order of magnitude at both stations, with less variability during summer months than in winter months. These features persist

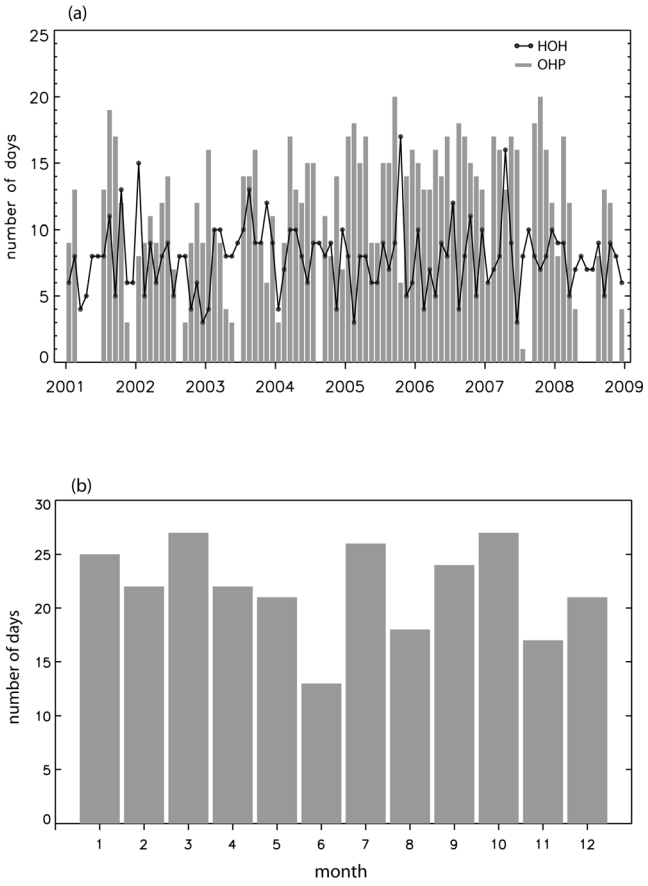

Figure 2. (a) Number of days per month with measurements at Observatoire de Haute Provence (OHP) (bars) and Hohenpeissenberg Observatory (HOH) (line) and (b) total number of days per month for the period 2001–2008 for which there were coincident measurements at both stations.

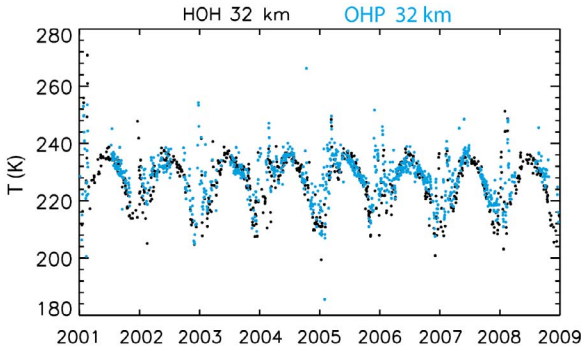

Figure 3. Daily temperature time series at 32 km from OHP (blue) and HOH (black) stations.

even when taking only measurements on coincident nights, suggesting that these differences have true geographical origin rather than being an effect of temporal sampling or instrument discrepancies. We next take a closer look first into the lidar-AMSU correspondence, and follow to use AMSU as a referential to compare T measurements at both stations.

3. Annual Cycle and Temperature Anomalies

[12] The first step is to relate AMSU and lidar measurements by establishing a correspondence between lidar heights and satellite channels. To this purpose we compare the annual cycles derived from each device (lidar and AMSU) at each station, following *Funatsu et al.* [2008]. The idea is to match a lidar altitude and AMSU channel by choosing the altitude that has the smallest annual mean absolute difference between AMSU and lidar temperatures. We chose not to average vertically the lidar profiles (with the AMSU weighting functions)

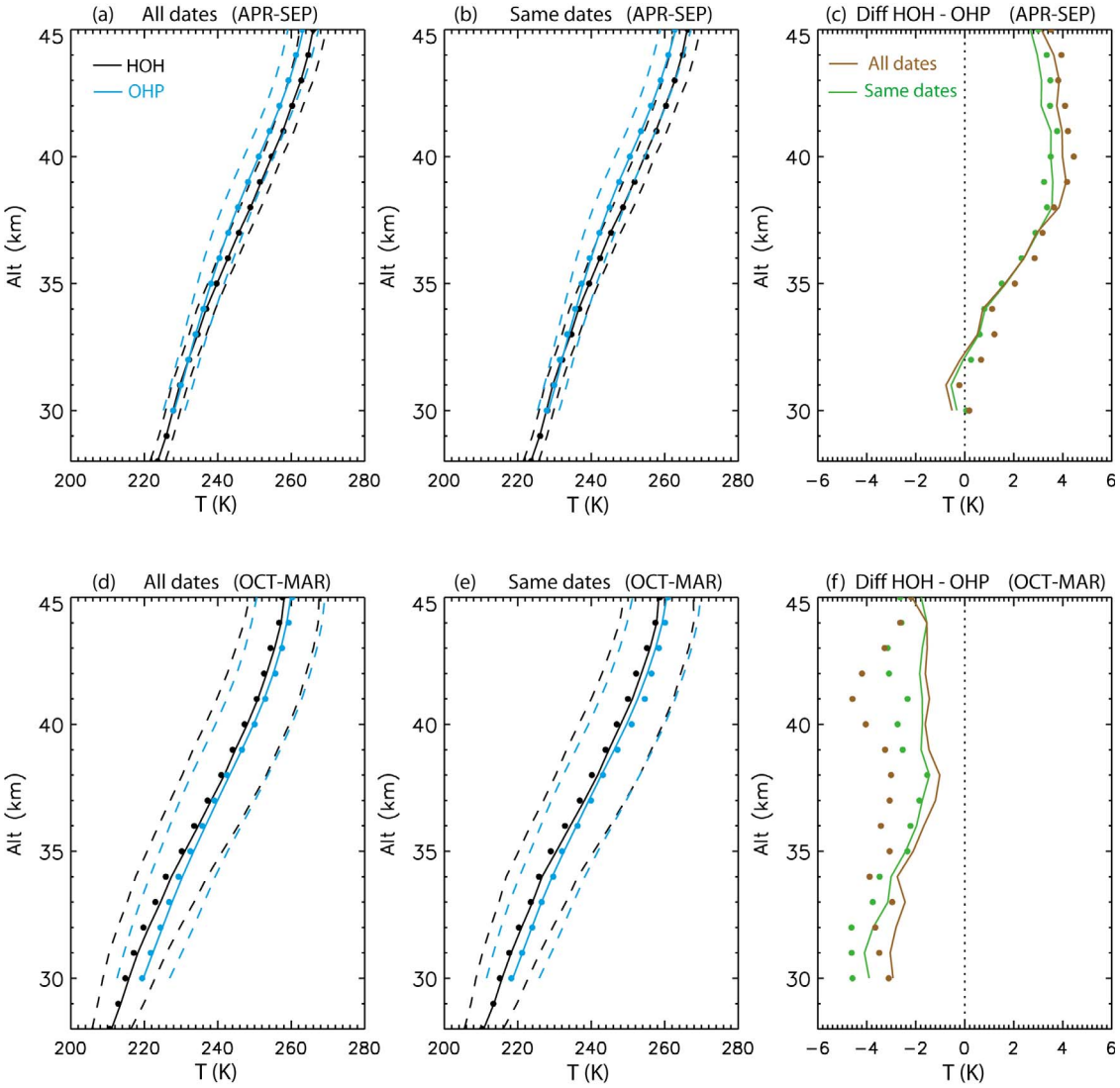

Figure 4. Six-month average vertical profiles (solid) and standard deviation (dashed), and median values (circles) at OHP (blue) and HOH (black) for (a and d) all available measurements at each lidar station and (b and e) only data from coincident nights. Difference between HOH and OHP mean (solid) and median (circles) measurements for (c) April through September and (f) October through March.

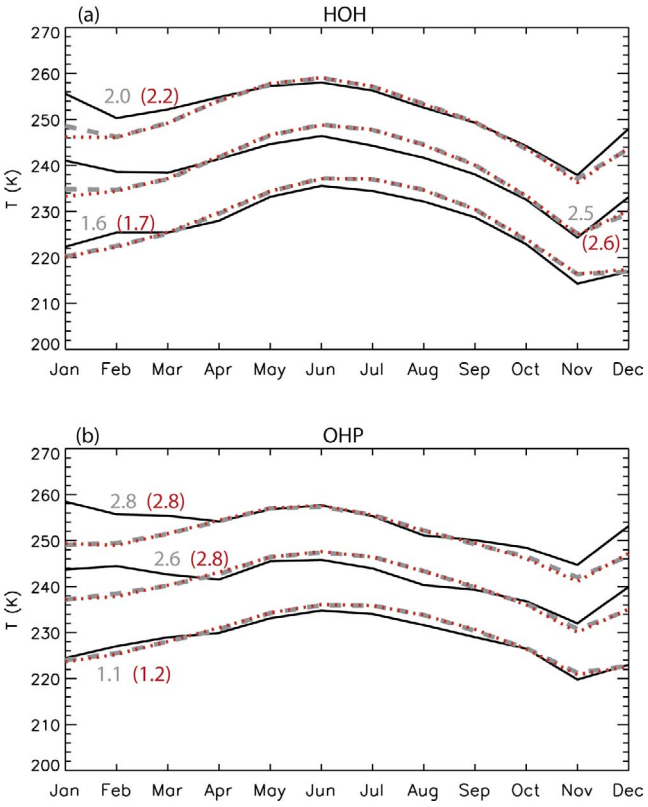

Figure 5. Lidar (black) monthly mean temperature annual cycle for selected altitudes of (a) HOH (32, 36, and 40 km) and (b) OHP (32, 37, and 41 km), with superimposed AMSU-A brightness temperature annual cycle based on available (red dot) and lidar coincident (gray dash) night passes. Numerical values represent the mean absolute temperature difference between lidar and corresponding color-coded AMSU averages.

because lidar uncertainty grows fast with altitude and not similarly for both lidars. Moreover, both lidars cover altitudes of ~30 km and higher, while AMSU channel 12 (and somewhat channel 13) has significant contribution from levels below this altitude. Another issue is that AMSU weighting functions vary slightly with season and latitude, which would add to the measurement uncertainties.

[13] Figure 5 shows the annual cycle of temperature for selected altitudes derived from OHP and HOH lidars and AMSU-based brightness temperatures using lidar-nights coincident passes and all nights. The annual mean difference increases slightly when all-nights AMSU is used to calculate the annual cycle. Overall the largest differences over the annual cycle are found in winter, where AMSU usually reports lower temperature than the lidars. This is the season that presents the strongest stratospheric temperature variability (e.g., Figures 4d and 4e). This variability is not entirely captured by AMSU because of the smoothing nature of the broad weighting functions and will be further discussed later on. The selected altitudes for OHP do not differ significantly from those in the work of *Funatsu et al.* [2008] that chose altitudes of 32, 36 and 40 km in their study (corresponding to mean absolute differences of 1.3, 2.7 and 2.7 K, respectively). The small discrepancies between the present and previous choices arise because the target area in the latter was slightly to the north, the period considered was 1 year shorter (2001 to 2008), and a compromise between AMSU, lidar and operational reanalysis data was sought.

[14] After selecting the combination of lidar heights matched to the AMSU channel, we derived a time series of temperature anomalies (T′) by removing the 8 year monthly mean value from the original daily time series; the resulting T′ time series are shown in Figure 6. It is evident from the time series that the T′ range observed by lidars is larger than those by AMSU, likely because of the smoothing inherent to the vertical and horizontal satellite measurements, as previously discussed by *Funatsu et al.* [2008]. These discrepancies are not mainly due to noise effects because T′ values far exceed the noise level especially in wintertime.

[15] Both sites show large T′ in wintertime that are a response to the upward propagating planetary waves with periods larger than 1 week [*Hauchecorne et al.*, 1991]. Such waves are blocked during spring and summer when winds in the lower stratosphere are predominantly from the east [*Hauchecorne and Chanin*, 1983]. This can be seen more clearly in T′ for the core winter months (December through February) as shown in Figure 7. Lidars and AMSU show that T′ variability is dominated by low-frequency (and synoptic) dynamics. Major stratospheric sudden warming (SSW) events are marked as "W" [*Charlton and Polvani*, 2007; *Manney et al.*, 2005; *Liu et al.*, 2008; *Manney et al.*, 2008]. It is interesting to notice that in some cases (February 2002, January 2003) there were negative T′s during SSW events, clearly indicating the zonal asymmetry of the dynamical perturbation.

[16] The next step was to examine how well lidar and AMSU measurements compare by analyzing their distributions (Figure 8); the corresponding standard deviation, kurtosis and skewness are given in Table 1. In general, both lidar and AMSU T′ distributions are monomodal but with flatter peak in the cold season, indicating higher thermal winter variability. There is also a considerable interannual variability (not shown) with some years with flatter distribution (2002, 2003) and others with a dominant peak (2001, 2008), reflecting the dynamical variability (and to some extent the uneven temporal sampling). AMSU T′ has higher kurtosis in winter than lidar, and shows larger interannual variability at HOH than at OHP. The smaller range of AMSU T′ is attributed to the "vertical smoothing" by the instrument's weighting functions that smoothes local temperature anomaly "peaks." While the lidar data are representative of a layer of 3 km, AMSU gives integrated information over a much deeper layer, which can lead to large differences. Because temperature variations at different atmospheric levels may exhibit anticorrelations the vertical smoothing tends to reduce anomalies. The T′ distributions at different locations exhibit very similar behavior in terms of shape and spread; however, the spread of AMSU@OHP in summer is markedly smaller than that of lidar at this station.

[17] Finally, we examine the linear relationship between lidar and AMSU observations. We find that they are well correlated (significance above 99%) particularly in the cold season with values around and above 0.8 (Figures 9g–9l). This high correlation value reflects the low-frequency dynamics variability captured by lidars and AMSU, as shown previously in Figure 7. While they are weaker in the warm

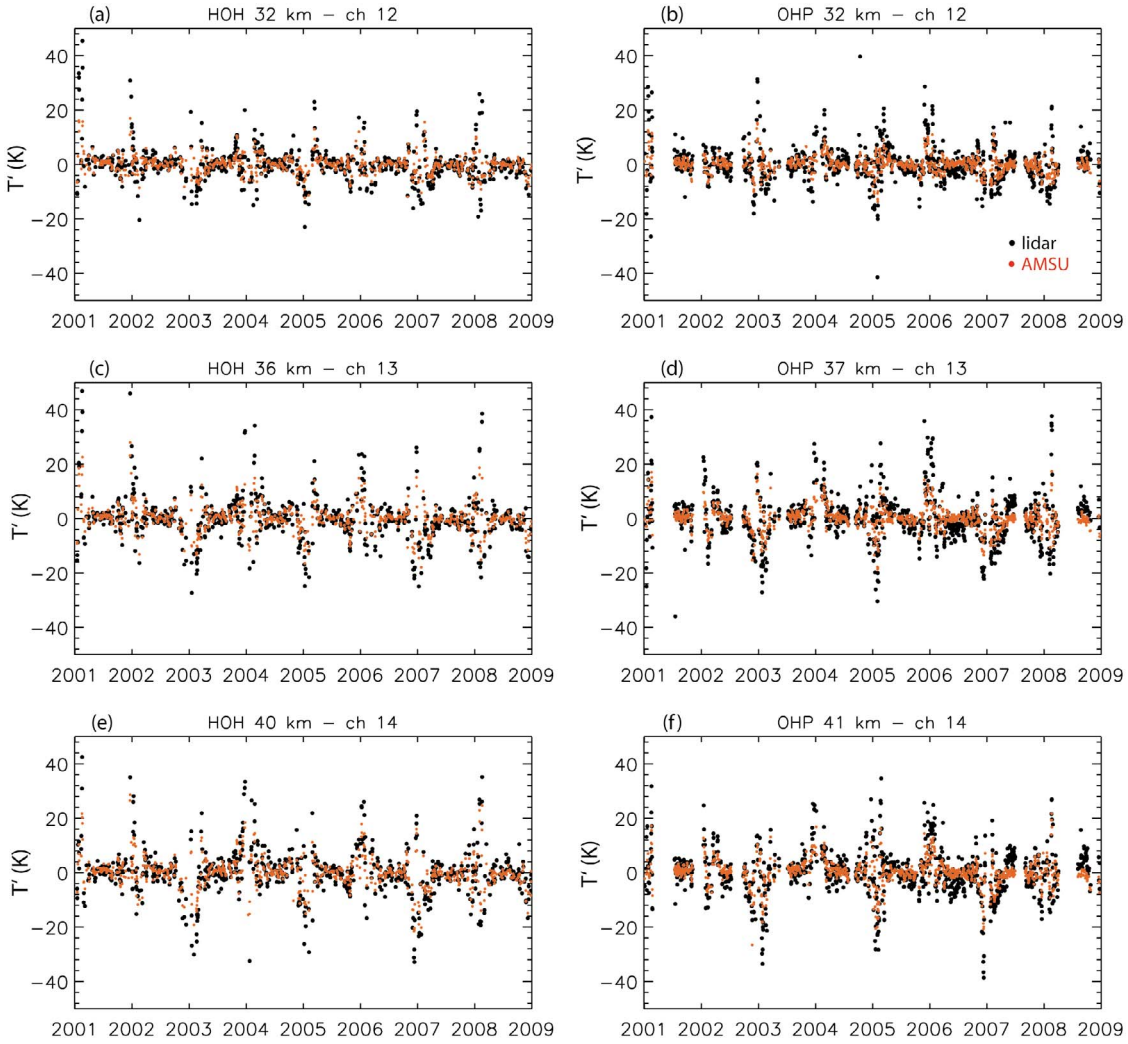

Figure 6. Daily temperature anomalies (black) (relative to mean annual cycle) time series at the (a, c, e) Hohenpeissenberg and (b, d, f) Observatoire de Haute-Provence stations and superimposed AMSU T anomalies (red).

season (Figures 9a–9f), they are higher at HOH (above 0.6) but relatively low at OHP (correlation of 0.5 or less). The decrease in correlation during summer is not entirely surprising as it was shown that AMSU@OHP T′ have much smaller spread than lidar T′s. In summer lidar T′ spread at OHP is larger than HOH, and much larger than that at AMSU@OHP. It is possible that the variability observed at OHP is due to a more local variability such as the effect of gravity waves (GW). Such effect is more evident in summer since T′ is generally low in summertime [*Wilson et al.*, 1991]. In winter T′ is dominated by large-scale planetary waves masking partially the effect of gravity waves [*Hauchecorne et al.*, 1991]. Possible sources of gravity waves include convective clouds, geostrophic adjustment of the jet stream, and mountainous chains [*Fritts and Alexander*, 2003]. Clearly both sites can be (and are) affect by GWs but OHP lidar could be more sensitive to its influence. Analysis of individual profiles for dates that showed a large discrepancy between the two sites measurements did not allow an unambiguous distinction between noise and GW signatures. Summertime data is more affected by the fact that there is less darkness (at both sites) as well as effects of longer integration time and haze at OHP, probably increasing the noise levels. The large power difference between the lidars would make it difficult to compare the GW activity (e.g., to analyze cutoff values for noise) at each site. Detailed investigations on the GW frequency and activity in summertime at these stations should be pursued as a new lidar with improved capability is to be installed at HOH; at this point we can merely point GW as a dynamical reason that could explain part of the observed discrepancies.

4. Differences in T Anomalies and Trends: Are They a Real Atmospheric Signature?

[18] While in section 3 we focused on the lidar-AMSU correspondence at each station, in the present section we focus on the lidar-lidar and AMSU-AMSU (at different stations) correspondences.

[19] In a first step, we examined the differences in the annual cycles at HOH and OHP (Figure 10a) corresponding to the differences in the annual cycles presented in Figure 5.

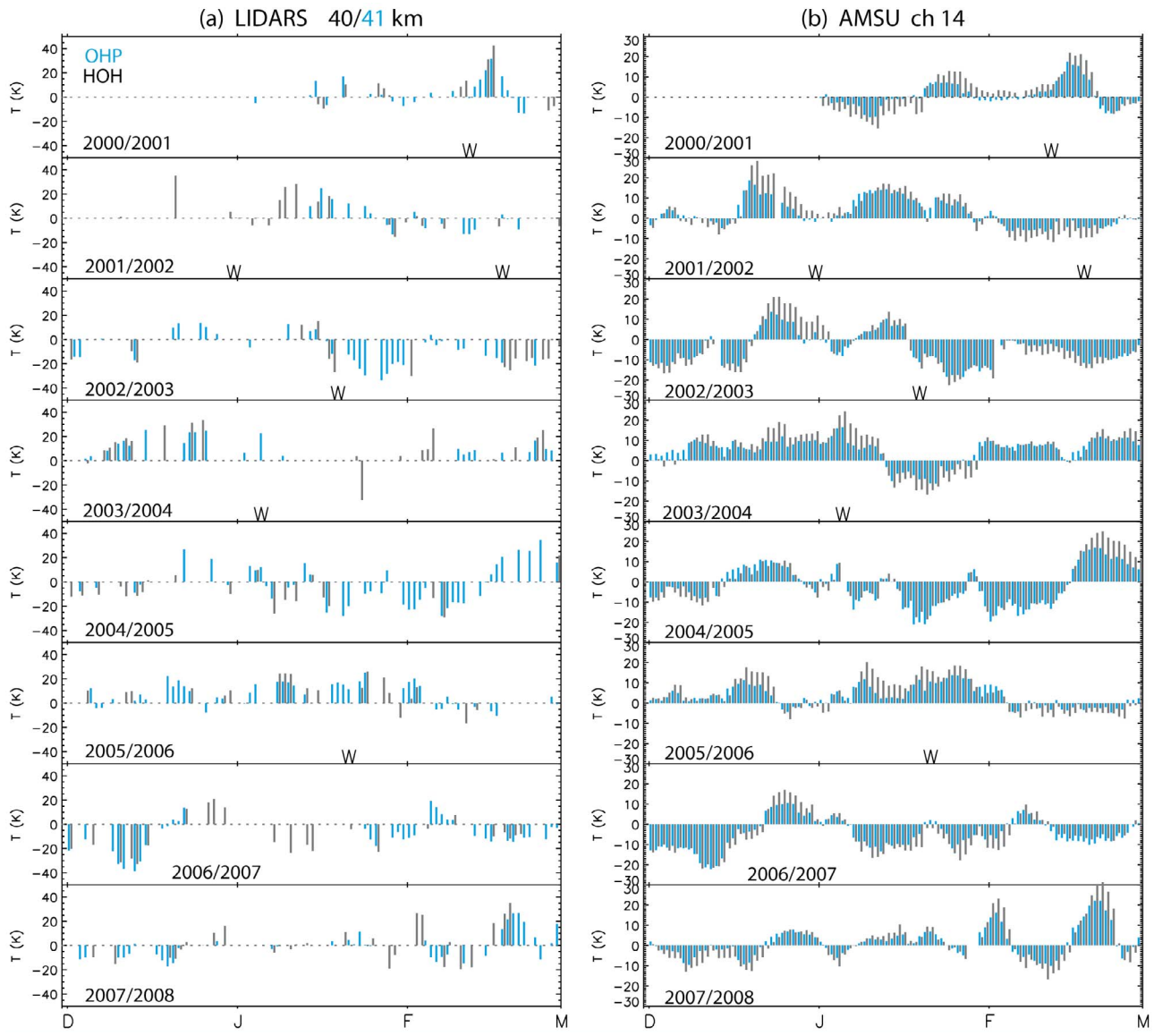

Figure 7. Daily temperature anomalies (relative to mean annual cycle) time series for December, January, and February between 2001 and 2008 at OHP (blue) and HOH (gray) as observed by (a) Lidars at 40/41 km and (b) AMSU channel 14. Central dates of major stratospheric sudden warming events are marked as "W."

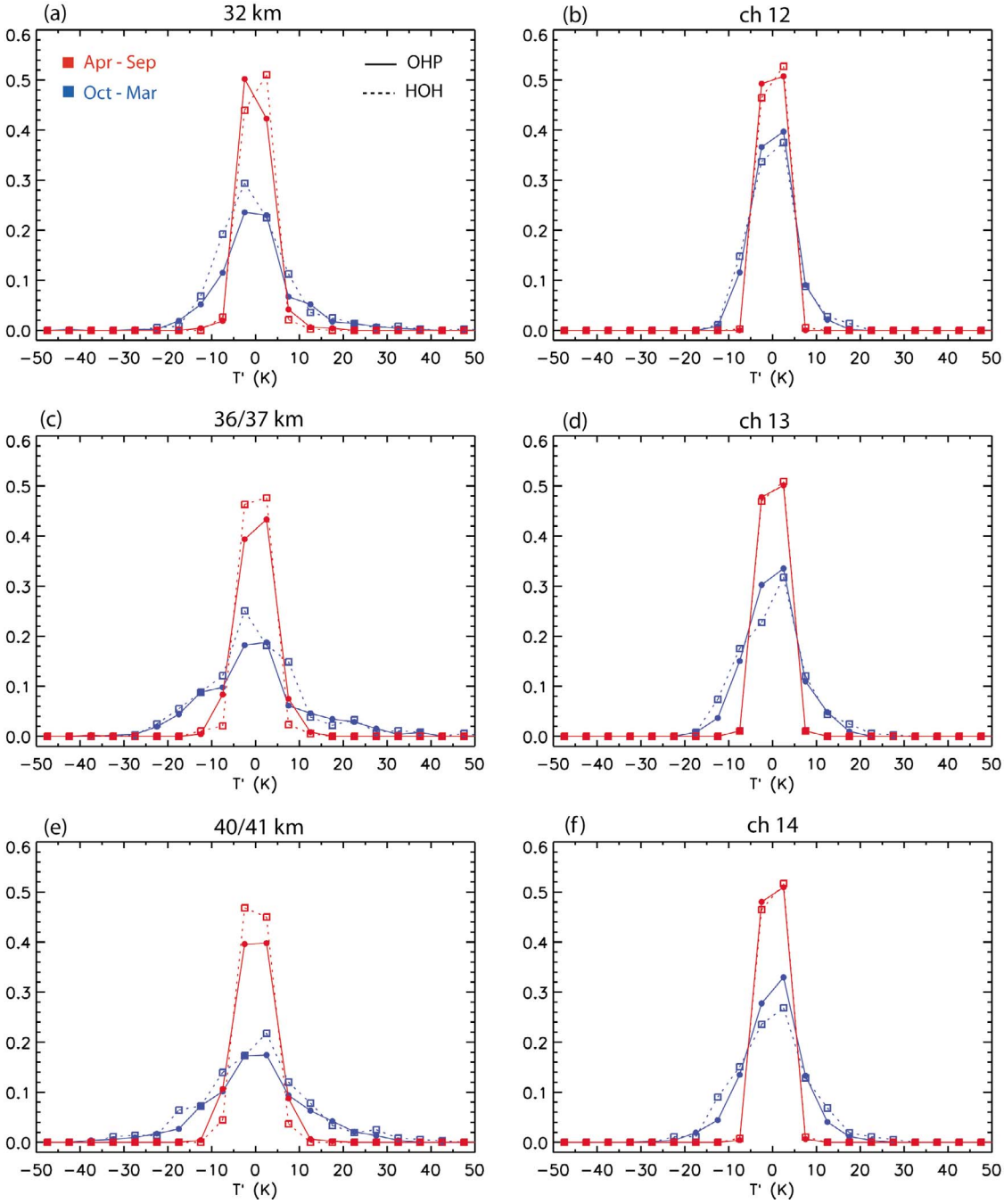

Figure 8. Summer and winter distributions of temperature anomalies of (a, c, e) lidar and (b, d, f) AMSU for OHP (solid) and HOH (dotted) stations.

Table 1. Standard Deviation (K), Kurtosis and Skewness of Lidar and AMSU-A (in Parentheses) T′ Distributions Shown in Figure 8[a]

	Standard Deviation		Kurtosis		Skewness	
	Lidar OHP (AMSU@OHP)	Lidar HOH (AMSU@HOH)	Lidar OHP (AMSU@OHP)	Lidar HOH (AMSU@HOH)	Lidar OHP (AMSU@OHP)	Lidar HOH (AMSU@HOH)
			Channel 12[b]			
Apr–Sep	3.1	2.4	5.0	5.0	2.6	2.6
	(1.4)	(1.6)	(4.8)	(5.0)	(2.6)	(2.6)
Oct–Mar	8.7	8.9	2.1	1.6	1.9	1.7
	(4.4)	(5.0)	(3.8)	(3.3)	(2.3)	(2.2)
			Channel 13[c]			
Apr–Sep	4.1	3.0	4.4	4.8	2.4	2.6
	(1.6)	(1.9)	(4.8)	(4.9)	(2.6)	(2.6)
Oct–Mar	10.9	11.6	1.1	1.2	1.5	1.5
	(5.9)	(7.1)	(2.7)	(2.1)	(2.0)	(1.8)
			Channel 14[d]			
Apr–Sep	3.9	2.8	3.9	4.7	2.3	2.5
	(1.7)	(1.9)	(4.8)	(4.9)	(2.6)	(2.6)
Oct–Mar	10.8	12.0	0.7	0.5	1.4	1.3
	(6.7)	(8.1)	(2.6)	(1.1)	(2.0)	(1.6)

[a]AMSU, Advanced Microwave Sounding Unit; OHP, Observatoire de Haute Provence; HOH, Hohenpeissenberg Observatory.
[b]Altitude = 32 km.
[c]Altitude = 36/37 km.
[d]Altitude = 40/41 km.

A very clear pattern can be seen in all curves: from mid-April through September, the lower stratosphere and midstratosphere at HOH is on average warmer than at OHP (positive differences in T), while during the remaining of the year, T is lower at HOH. Because these features are consistent regardless of temporal sampling (and consistent with the seasonal average depicted earlier in Figure 4 for lidars only), and appears also using AMSU at both locations, it suggests again that the dissimilarities on the measurements are of geophysical origin. All three levels/channels show a minimum in November–December, whereas the upper stratospheric channels (13 and 14) present an additional minimum in February. The relative maximum in December–January in the two upper levels/channels appeared because there was relatively more sampling of warm (with respect to its climatological monthly mean value) than cold days in these months in this region (Figure 7). For channel 12, which has significant contributions from altitudes both above and below 30 km (see Figure 1), the warm/cold amplitudes were less accentuated and smeared out the secondary minimum (not shown). HOH is geographically closer to the winter polar vortex than OHP, explaining the negative wintertime values. Climatologically HOH is slightly warmer in summer than OHP at the altitudes considered [e.g., *Andrews et al.*, 1987] resulting in positive differences in this season.

[20] These temperature difference patterns also appear in the Committee on Space Research (COSPAR) International Reference Atmosphere (CIRA-86) [*Fleming et al.*, 1990] (http://badc.nerc.ac.uk/data/cira/) data, as can be seen in Figure 10b. This figure shows 80% of the zonally averaged temperature difference between 50°N and 45°N (since the latitude difference between OHP and HOH is of 4°) at 3.224 hPa (about 39.4 km) from the CIRA-86 temperature tables. It clearly shows that CIRA-86 reproduces the double minimum seen by the lidars in November–December and in February with a relative maximum in January. These features are likely related to the evolution of SSWs that occur preferentially in January–February [e.g., *Charlton and Polvani*, 2007], and also appear in the zonally averaged monthly mean AMSU data at channel 14 (not shown). However, the amplitude in CIRA-86 is not as large as in lidar data and there is probably an additional regional effect. A possible cause is the average displacement of the polar vortex in the direction of Scandinavia leading to a larger temperature latitudinal gradient above Europe than at other latitudes.

[21] Furthermore, these results confirmed that AMSU based on coincident dates with lidar (compare solid and dashed lines) have a more consistent behavior with the ground-based measurements than AMSU based on all measurements, particularly in wintertime. For example, lidars present at 36 and 40 km a sharp T decrease between January and February, and increase between November and December, which are well mimicked by the AMSU counterpart using coincidental dates, but less so when the average of all nights for AMSU are used. During summer, the temporal sampling issue is less evident for AMSU-based annual cycles (compare dashed and dotted lines between mid-April to September).

[22] Now we compare lidar and AMSU data based on coincident dates at both sites, to narrow the focus on geographical and instrumental differences. Furthermore because AMSU@OHP and AMSU@HOH use the same instrument, their differences reflect the vertically averaged geophysical effect when using coincident dates only. We proceeded to examine the correlation between T′s measured by lidars at the two stations and by AMSU at each station. The correlation r_{Lidar} between the two lidars is high in winter despite the difference in instruments (0.86, 0.91, and 0.90 with increasing altitude; Figures 11g–11i); however, correlation is decreased in summer (0.46, 0.48 and 0.39 with increasing altitude; Figures 11a–11c). The red crosses in Figures 11g–11l represent dates within ±10 d of a reported major SSW. In most instances T′ at each station had the same sign but different amplitudes, and in few cases T′ was much larger at HOH than at OHP. AMSU measurements targeting different

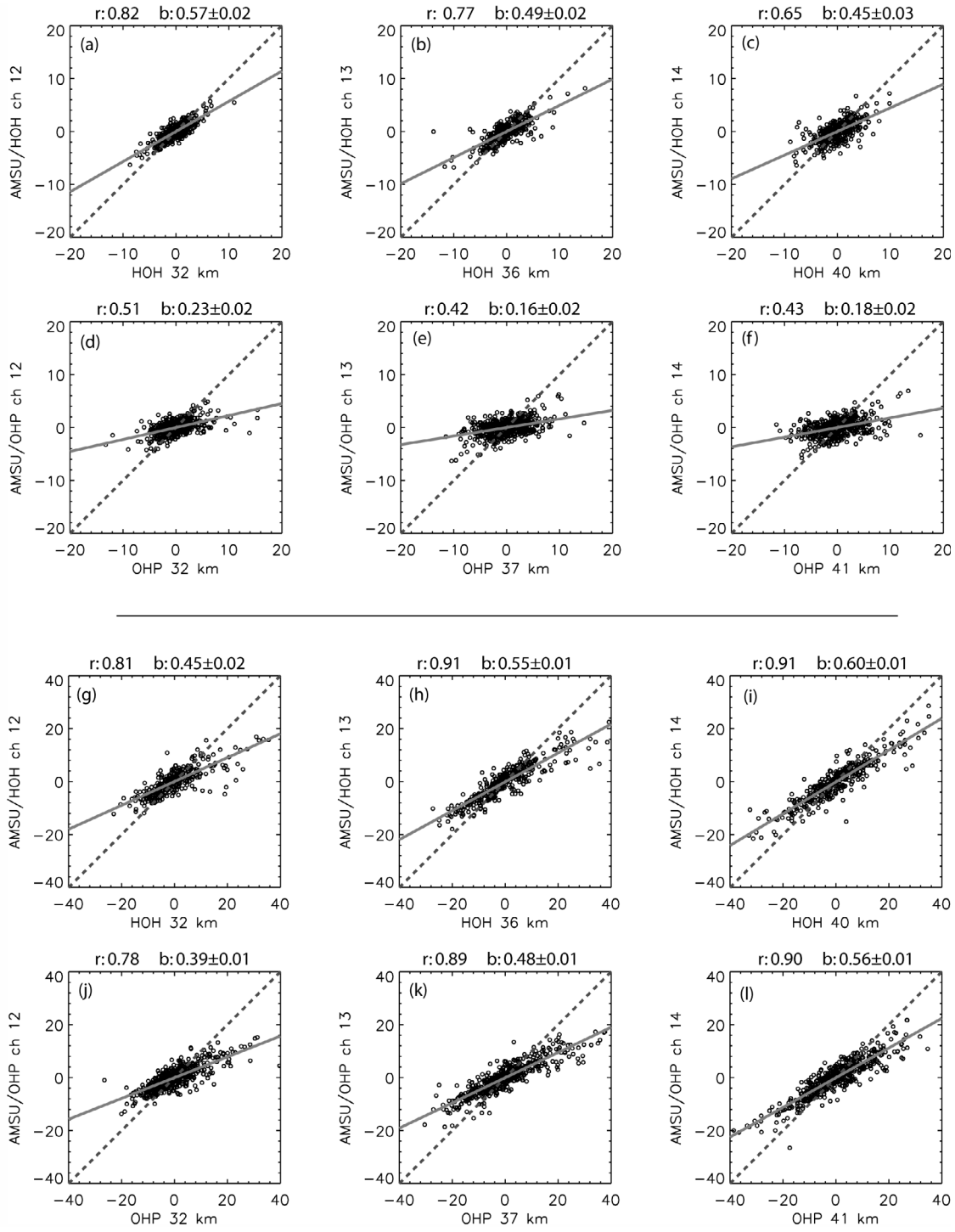

Figure 9. Least squares fit (gray line; slope and uncertainty given by "b" at the top of each panel) between HOH and AMSU@HOH T′ (K) at (a, g) 32 km/channel 12, (b, h) 36 km/ channel 13, and (c, i) 40 km/ channel 14 and OHP lidar and AMSU@OHP at (d, j) 32km/ channel 12, (e, k) 37 km/ channel 13, and (f, l) 41 km/ channel 14, and respective linear correlation (r) values. Figures 9a–9f correspond to the period April through September (summer), while Figures 9g–9l represent the period October through March (winter); notice the change in the temperature range for the two seasons.

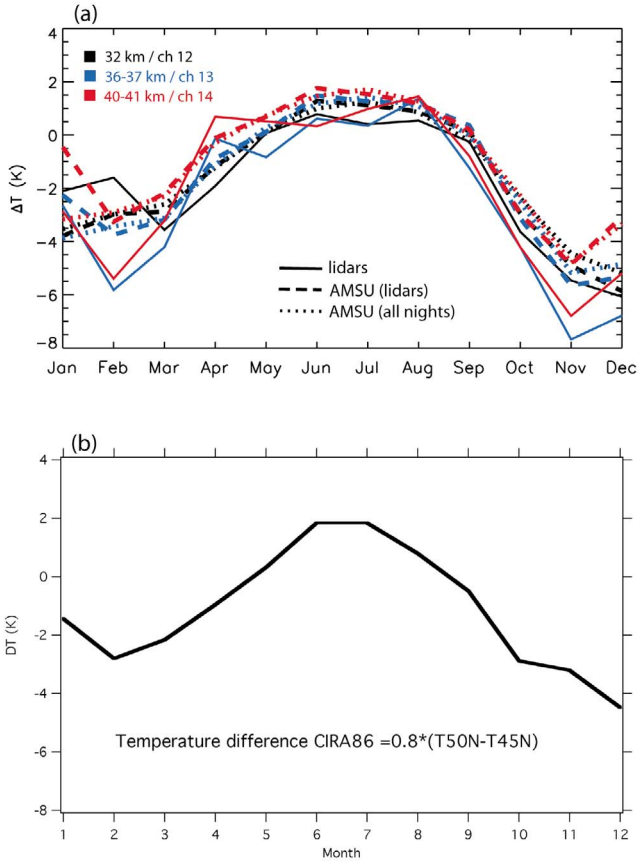

Figure 10. (a) Differences between annual cycles at HOH and OHP: solid line for lidars, dashed for AMSU measurements using coincident lidars only, and dotted for all AMSU measurements; (b) CIRA-86 model temperatures at 3.224 hPa.

regions only 5° apart have consistently good correlation (r_{AMSU}) between 0.93 and 0.95 throughout the year (Figures 11d–11f and Figures 11j–11l). Although the satellite instrument is identical and T′ is based on coincident dates, it is tempting to attribute a correlation slightly smaller than 1 to noise. Noise plays a role in decreasing correlation; however, preliminary analysis comparing temperature time series of NOAA-15, 16 and 18 for these channels show that correlations between brightness temperature series of same instruments in different platforms (measuring an identical region in the midlatitudes) can reach 0.99 (not shown) suggesting that noise contributes little to reduce the correlation. In fact, the value of $r_{AMSU} \sim 0.94$ should be considered relative to the value of $r_{Lidar} \sim 0.90$ (winter) or $r_{Lidar} \sim 0.45$ (summer). The values of interest are $(r_{AMSU} - r_{Lidar})/(1 - r_{Lidar}) \sim 0.04/0.10 = 0.40$ in winter, and $(r_{AMSU} - r_{Lidar})/(1 - r_{Lidar}) \sim 0.49/0.55 = 0.90$ in summer. This means that in winter, around ~60% of the differences between T′ are due to geophysical effects and ~40% due to instrument differences. The geographical/geophysical effect has a non-negligible impact on T′ values. In summer the decorrelation due to geophysical effects is estimated to account for ~10%.

[23] Further insight is gained by analyzing the T′ distributions of lidars and AMSU for coincident dates only, as shown in Figure 12. It is interesting to notice that during summer, lidar measurements at OHP cover consistently a higher range than HOH at altitudes below 37 km, while both AMSU@OHP and AMSU@HOH distributions show similar median, interquartile range and skewness (that is, similar distribution location, spread and shape). On the other hand, at 40–41 km, both lidars and AMSU at different stations have similar distributions. As seen in section 3, AMSU and lidar measurements at OHP are not well correlated in summer; it is not clear whether the differences in the measurements are due mainly to location or to instruments. However, in wintertime (Figures 12d–12f) AMSU@HOH and AMSU@OHP have slightly different distributions: AMSU@OHP has narrower spread (and is less skewed at channel 14) than AMSU@HOH. These features are also observed in the distributions of measurements by lidar at each station (and is also represented with the slope of OHP versus HOH smaller than 1 in Figures 11g–11i), supporting the argument for geophysical effect as the main cause of the temperature measurement discrepancies in this season.

[24] Finally, we present the T′ tendencies at both stations as inferred from both lidar and AMSU measurements. The term "tendency" is used here instead of "trend" since the short data time span prevents strict trend calculations. To calculate these tendencies we first produce monthly mean T′ time series (for lidars and AMSU) based solely on coincident night measurements, and then we perform linear regression. Note that because of the small number of coincident night measurements such monthly means could be based on one or two dates per month; that means that their absolute value is not realistic and should be regarded only in relative terms. There is a fairly good agreement between the lidar and AMSU monthly means at both stations, as seen in Figure 13. Besides tendencies for coincident dates only, Table 2 presents as well tendencies for monthly means at each station using all available measurements at each site for lidar and AMSU, as well as for AMSU using all night measurements available. All tendencies and their uncertainties are very large (compared to long-term trend estimates) because of the short time series but their values can still be compared with each other to examine the geophysical, instrumental and temporal effect on these estimates.

[25] Individual lidar T′ tendencies at HOH and OHP (using all lidar measurements at each station) present cooling at both sites at all levels; however, it is stronger at HOH, around −4 K/decade compared to −2 to −3 K/decade at OHP. Tendencies at OHP are comparable to estimates for the period 2001–2007 [*Funatsu et al.*, 2008]. Such estimates are very different from trends derived for the period 1988–2005 [*Randel et al.*, 2009] where both OHP and HOH present warming trends up to 37 km; above this level HOH trends are still positive while OHP trends are slightly negative. Tendencies estimated using corresponding AMSU night measurements corroborates the recent cooling tendencies (however, there are large uncertainties because of the short time period considered).

[26] Tendencies estimates using only coincident dates show a stronger cooling at HOH (from ~−4 to −7 K/decade) than at OHP (from ~+1 to −4 K/decade) at all levels. Similarly, BT′ tendencies for coincident nights indicates cooling ranging from ~−2 to −5 K/decade at OHP, while at HOH the cooling is stronger, around −3 to −6 K/decade. AMSU estimates using all available nighttime measurements show a similar relative result, with slightly stronger cooling at HOH

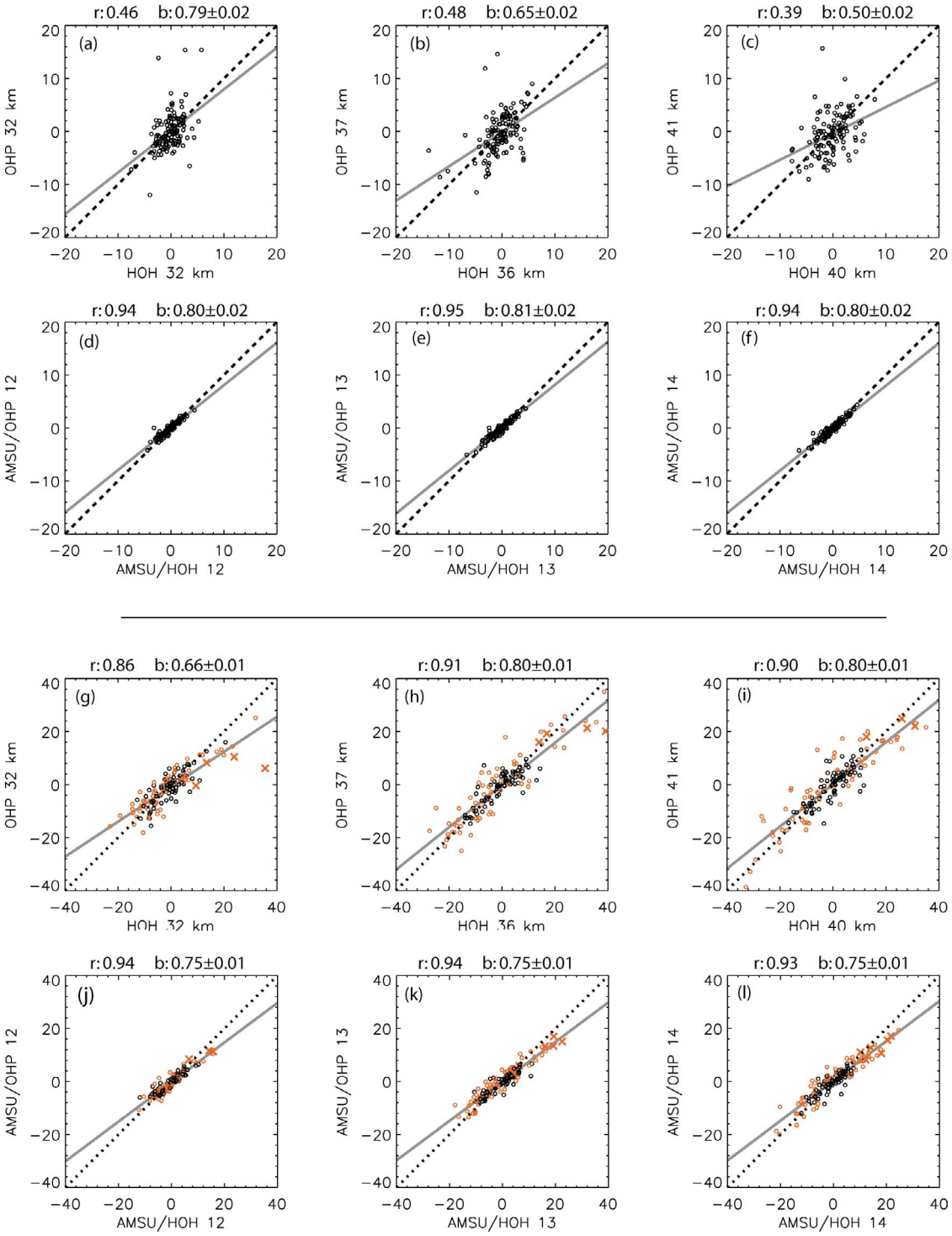

Figure 11. Least squares fit (gray line; slope and uncertainty given by "b" at the top of each panel) between OHP versus HOH lidar T′ at (a, g) 32–32 km, (b, h) 37–36 km, and (c, i) 41–40 km and AMSU@OHP versus AMSU@HOH BT′ for (d, j) channel 12, (e, k) channel 13, and (f, l) channel 14 and respective linear correlation (r) values. Figures 11a–11f correspond to the period April through September (summer), while Figures 11g–11l represent the period October through March (winter); notice the change in the temperature range for the two seasons. Winter values for December, January, and February are represented in orange; "x"s denote dates within ±10 d of the central date of a major sudden stratospheric warming occurrence during the period.

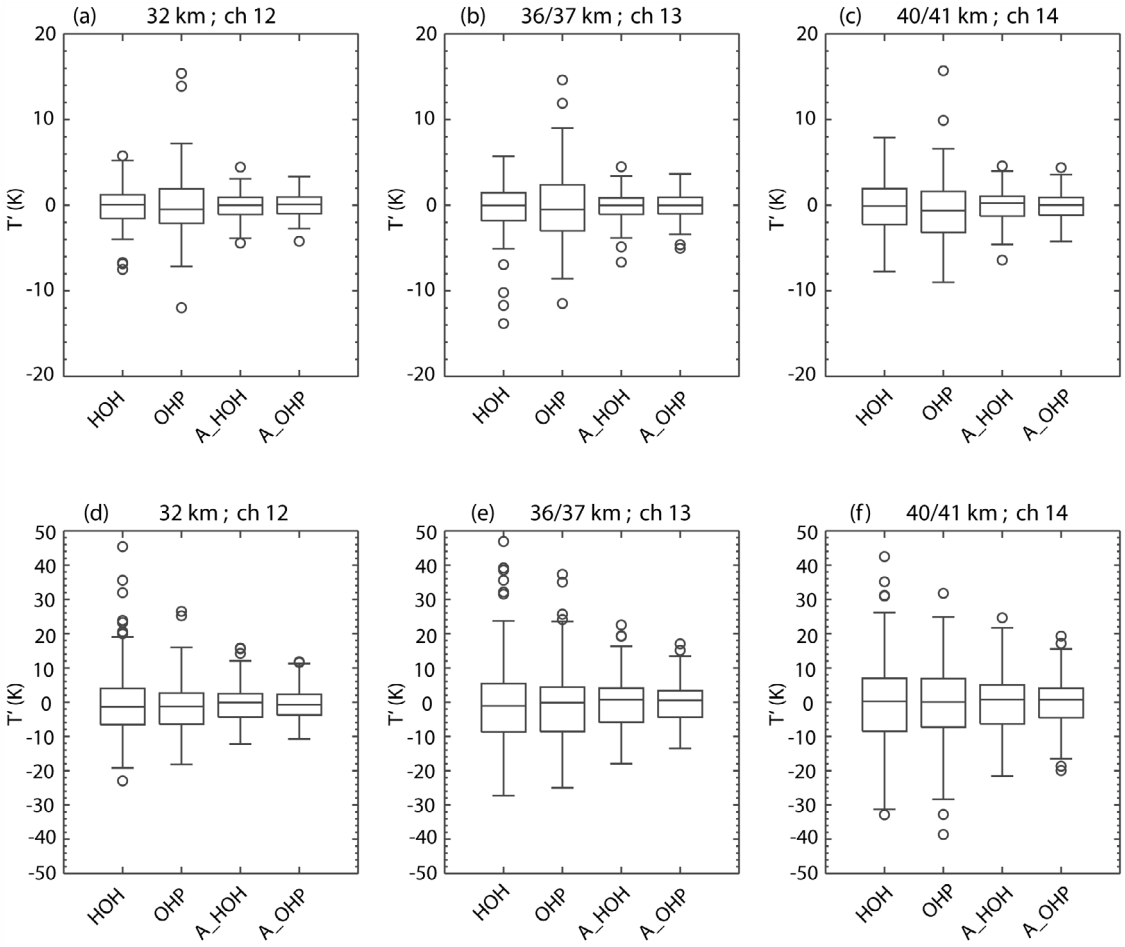

Figure 12. Temperature anomaly distributions of coincident measurement nights at HOH, OHP, AMSU@HOH, and AMSU@OHP. Corresponding altitudes and channels are shown on top of each panel for (a–c) summer and d–f) winter seasons. Whiskers define the lowest datum still within 1.5 of the interquartile range (IQR) of the lower quartile and the highest datum still within 1.5 IQR of the upper quartile; circles denote outliers. Note here that the vertical scales are different for summer and winter seasons.

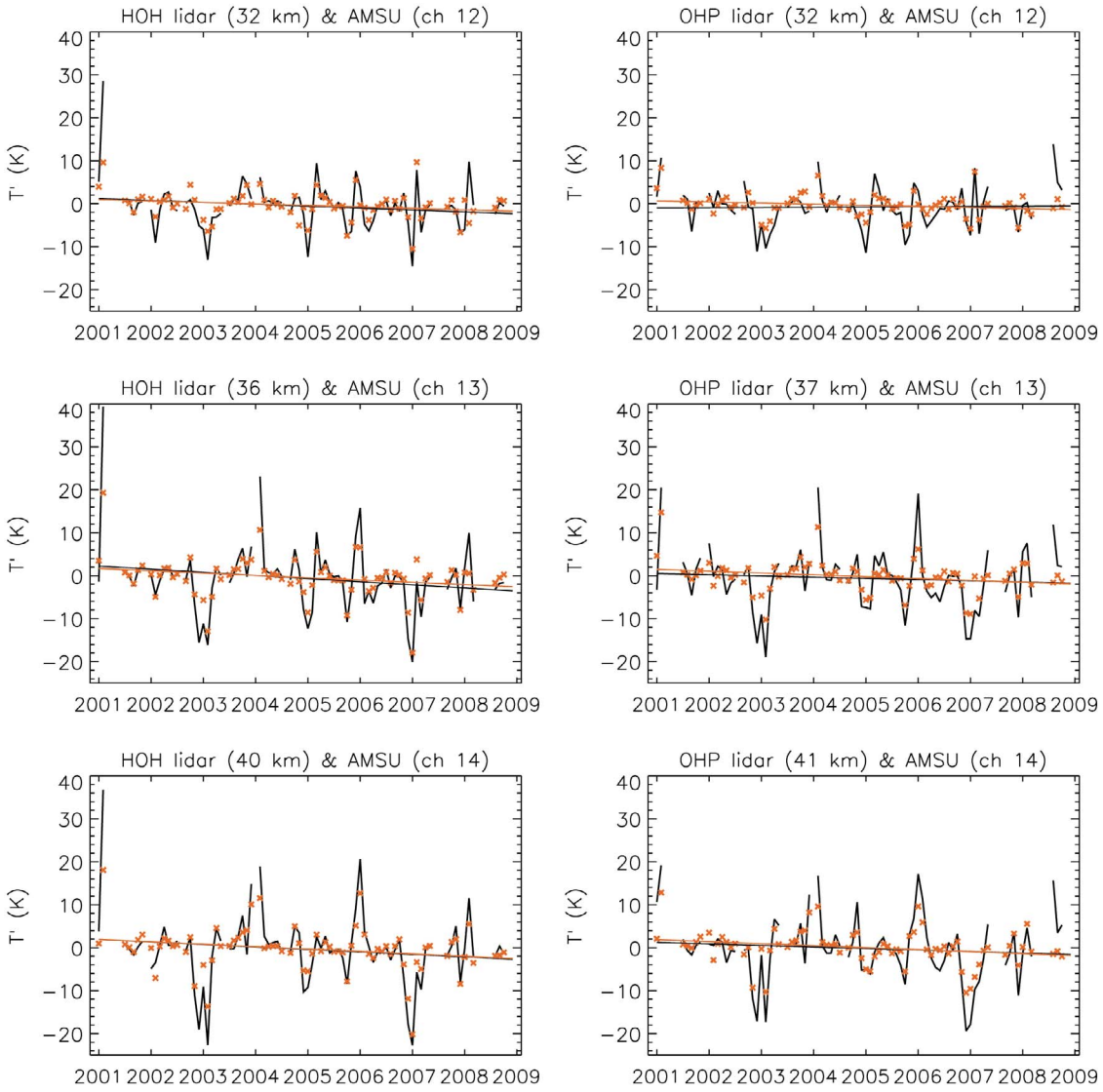

Figure 13. Lidar (black) and AMSU (red) monthly mean T′ time series for (left column) HOH and (right column) OHP for the altitudes and channels indicated on top of each panel. Simple linear regression fit for each series is superimposed with same color key.

Table 2. Coefficients of Linear Regression of Monthly Mean Temperature Anomalies With Respect to Time for the Period 2001–2008[a]

	AMSU		Lidar		
Channel	OHP	HOH	Altitude	OHP	HOH
		Lidar Nights (At Each Station)			
ch 12	−3.1 ± 0.9	−2.4 ± 1.0	32 km	−2.7 ± 1.8	−4.5 ± 1.7
ch 13	−3.7 ± 1.5	−3.7 ± 1.5	37/36 km	−3.0 ± 2.9	−5.7 ± 2.4
ch 14	−3.5 ± 1.7	−4.1 ± 1.7	41/40 km	−2.0 ± 2.6	−3.8 ± 2.5
		Coincident Nights			
ch 12	−2.6 ± 1.4	−3.4 ± 1.7	32 km	+0.6 ± 2.5	−4.4 ± 3.0
ch 13	−4.3 ± 2.0	−5.3 ± 2.5	37/36 km	−2.8 ± 3.8	−7.3 ± 4.3
ch 14	−4.7 ± 2.2	−5.6 ± 2.8	41/40 km	−3.6 ± 4.0	−5.8 ± 4.5
		All AMSU Overpasses			
ch 12	−1.7 ± 0.6	−2.4 ± 0.7			
ch 13	−2.5 ± 1.0	−3.2 ± 1.1			
ch 14	−2.7 ± 1.2	−3.3 ± 1.4			

[a]Tendencies and uncertainties (1-sigma) are given in units of K/decade.

than at OHP; the cooling rate is, however, about 30–40% weaker than using only coincident night measurements indicating the effect of subsampling on tendency calculation. AMSU-based tendency estimates using coincident dates point to nonnegligible geophysical distinctness between these two sites.

5. Discussion and Conclusions

[27] *Keckhut et al.* [2011] showed that trends calculated on the differences between OHP (HOH) and SSU channel 47X (peaking at about 1 hPa), that they termed "residual trends," have values as large as 0.6 ± 0.3 K (1.7 ± 0.6 K) for the period 1994 to 2004. They concluded that differences in residual trends at these lidar stations cannot be attributed solely to instrumental distinctiveness or changes. This finding was also corroborated by NCEP monthly data analysis, which indicated that these disparities could be representative of atmospheric variability. For example, the stratospheric temperature at HOH is colder in winter and warmer in summer than at OHP because of its more northern position; moreover they are located in latitudes where temperature gradients are strong and highly variable particularly in wintertime because of the wobbling of the polar vortex. The recent AMSU data, currently onboard NOAA-15 and higher platforms and MetOp satellites, is used here to further address this issue. *Funatsu et al.* [2008] showed that temporal and spatial sampling can have an effect on the estimation of tendencies (and consequently on long-term trends), therefore we use AMSU data targeting a region overpassing each station without overlapping with each other so that they are geographically isolated. In this manner, we can better separate the issues of instrument (by using AMSU for both locations), temporal sampling (by using only coincident dates with measurements at both stations) and geographical location (by "isolating" each target area).

[28] In order to obtain meaningful results, it is necessary that lidar and AMSU characterizations of the stratospheric temperature have good correspondence. Hence in a first step we compared lidar and AMSU at each station. We found that HOH temperature anomalies are highly correlated with AMSU@HOH throughout the year, with correlations ranging from 0.65 to 0.91 (correlation is dependent on season and height). OHP is highly correlated with AMSU@OHP in winter, with values larger than 0.78; however, correlation is noticeably weaker during summer, with values ranging from 0.42 to 0.51. One physical explanation for this decrease in correlation could be the local effect of gravity waves in summer. This hypothesis was not addressed in this study and should be further investigated as a more powerful lidar is to be installed at HOH. During winter temperature anomalies are dominated by planetary waves that have a large horizontal and vertical extension and are also well captured by AMSU. During summer planetary waves do not propagate in stratospheric easterly winds so that the effect of gravity waves is more prominent. AMSU@OHP may not be able to resolve for these anomalies since it is spatially averaged, hence the drop in correlation values (HOH also shows a slightly decreased correlation in summertime compared to wintertime). Nevertheless, both lidar and AMSU-based anomaly distributions at OHP and HOH have similar shape and spread, although AMSU measurements have a smaller T′ range because of the weighting function smoothing effect.

[29] We then proceeded to compare lidar at HOH and OHP, and AMSU at OHP and HOH using only coincidental lidar dates. In winter lidars measurements have good correlation despite their distinct instruments, ranging from 0.86 to 0.91; their correlation is weaker in summer, between 0.39 and 0.48. AMSU measurements have correlation up to 0.95 at all seasons. Such correlation is slightly higher than the "background" wintertime correlation of ~0.90, which is rather large considering that measurements are taken by very different instruments. The correlation differences between AMSU and lidar indicate that geophysical effects account for roughly 60% of the decorrelation in wintertime; in summertime this effect is reduced to about 10% only. The uncorrelated part could be due to differences in length of lidar measurements, noise due to haze, or dynamical effects such as gravity wave. Analysis of seasonal distributions of T′ for coincident night measurements further suggest that in winter both lidars at HOH and OHP, and AMSU@HOH and AMSU@OHP have analogous, slight differences, with larger spread at HOH measured by both ground and satellite instruments. There is thus strong evidence that at least in wintertime the differences in T′ have a stronger signature of the geophysical effects rather than instrumental differences. However, in summer, this distinction remains unclear, and more studies should be conducted to characterize the stratospheric variability in this season. Temperature tendencies also reflect the effect of geophysical differences: Estimates based on lidar measurements since 2001 show a stronger cooling at HOH than at OHP that is corroborated by AMSU analysis using coincident night measurements only and all available nights. Furthermore temporal subsampling of AMSU measurements resulted in a cooling between 30 to 40% stronger than using all available nights, which supports estimates obtained for OHP by *Funatsu et al.* [2008] for a slightly shorter period (2001–2007).

[30] The study presented here could be further extended with the use of reanalysis data, for example, separating SSW and non-SSW dates and then correlating T′ with potential vorticity-based equivalent latitudes for each case. Also, as mentioned earlier, further GW analysis should be performed to investigate their impact on temperature measurements in

Table 3. Linear Transformation Coefficients From Lidar T′ Anomalies to AMSU T′[a]

		OHP			HOH		
	Altitude/Channel	a	b	E	a	b	E
Apr–Sep	32 km/ch 12	0.00	0.23	0.02	−0.00	0.57	0.02
Oct–Mar		−0.02	0.39	0.02	0.03	0.45	0.02
Apr–Sep	36–37 km/ch 13	0.00	0.16	0.02	0.00	0.49	0.02
Oct–Mar		−0.03	0.48	0.01	−0.10	0.55	0.01
Apr–Sep	40–41 km/ch 14	0.00	0.18	0.02	−0.00	0.45	0.03
Oct–Mar		−0.02	0.56	0.01	−0.13	0.60	0.01

[a]The letter "a" is the linear regression constant (K), and "b" and "E" are the slope and uncertainty (1-sigma), respectively, of the linear transformation (nondimensional).

the summer season. Nevertheless the present analysis has important implications for example for strategies of satellite data used for stratospheric temperature monitoring, since spatial and temporal sampling play a role in determining trends [*Funatsu et al.*, 2008; *Steinbrecht et al.*, 2009b]. It shows that it is necessary to investigate the sensitivity of trend calculation based on zonally averaged data to the geographical location, since a small latitudinal shift (5° in the present case) can affect T′ distribution.

[31] Another point that we did not address in the present study is the issue of satellite drift: NOAA satellites have been undergoing significant drift causing the hours of overpasses over OHP and HOH to shift from around midnight to early morning. This drift has an effect on the calculation of tendencies, and was estimated to be around 1.5 and 3 K between the period 2004–2007 for monthly mean AMSU brightness temperatures over OHP [*Funatsu et al.*, 2008]. Because of the tidal effect (mostly important for channel 14) there is an inherent nonuniformity in the AMSU data that must be addressed. The high correlation between lidar and AMSU data in winter can be sought as an avenue to approach this problem, for example through a linear function ("transfer function") between AMSU and lidar temperatures. In a first approximation this transfer function could be used to "bring" the temperatures closer to the nighttime frame. The coefficients of the transformation $y = a + (b \pm E)x$, with y denoting lidar T′, x the AMSU BT′, a the linear fit constant, b the slope of the function, and E the uncertainty are given in Table 3 for summer and winter. These coefficients also offer a potential to perform intersatellite adjustments, as different NOAA (and MetOp) satellites have different equatorial crossing times and may present as well slight AMSU response differences. These results as well as a previous one addressing the sampling issues [*Funatsu et al.*, 2008] can be considered as a prestudy of a more ambitious project that consists in deriving accurate consistent temperature trends from the successive AMSU instruments in space. All the different issues (time sampling, orbit drift, time adjustment, and local variability) require the contribution from the lidar network to be addressed. In this present study, we have investigated the regional variability, anomaly distributions and show the high consistency between both measurement systems that renders such a project feasible.

[32] **Acknowledgments.** The lidar data used in this study were obtained as part of the Network for the Detection of Atmospheric Composition Change (NDACC) and are publicly available at http://www.ndacc.org. Measurements at OHP are carried out as part of a national observing system of the Institut National des Sciences de l'Univers (INSU) and is coordinated by the Observatoire de Versailles-Saint-Quentin (OVSQ-IPSL) with the additional support of CNES and ADEME. AMSU data were obtained through the French Mixed Service Unit ICARE. This work was performed under the framework of the European Integrated Project Geomon selected by the 6th Framework Program (contract FOP6-2005-Global-4-036677). We acknowledge the remarks of two anonymous reviewers that significantly improved the manuscript.

References

Andrews, D. G., J. R. Holton, and C. B. Leovy (1987), *Middle Atmospheric Dynamics*, 489 pp., Academic, New York.

Austin, J., et al. (2009), Coupled chemistry climate model simulations of stratospheric temperatures and their trends for the recent past, *Geophys. Res. Lett.*, *36*, L13809, doi:10.1029/2009GL038462.

Cagnazzo, C., C. Claud, and S. Hare (2006), Aspects of stratospheric long-term changes induced by ozone depletion, *Clim. Dyn.*, *27*, 101–111, doi:10.1007/s00382-006-0120-1.

Charlton, A. J., and L. M. Polvani (2007), A new look at stratospheric sudden warmings. Part I: Climatology and modeling benchmarks, *J. Clim.*, *20*, 449–469, doi:10.1175/JCLI3996.1.

Fleming, E. L., S. Chandra, J. J. Barnett, and M. Corney (1990), Zonal mean temperature, pressure, zonal wind and geopotential heights as function of latitude, *Adv. Space Res.*, *10*, 11–59, doi:10.1016/0273-1177(90)90386-E.

Funatsu, B. M., C. Claud, P. Keckhut, and A. Hauchecorne (2008), Cross-validation of Advanced Microwave Sounding Unit and lidar for long-term upper-stratospheric temperature monitoring, *J. Geophys. Res.*, *113*, D23108, doi:10.1029/2008JD010743.

Fritts, D. C., and M. J. Alexander (2003), Gravity wave dynamics and effects in the middle atmosphere, *Rev. Geophys.*, *41*(1), 1003, doi:10.1029/2001RG000106.

Gelman, M. E., A. J. Miller, K. W. Johnson, and R. M. Nagatani (1986), Detection of long-term trends in global stratospheric temperature from NMC analyses derived from NOAA satellite data, *Adv. Space Res.*, *6*, 17–26, doi:10.1016/0273-1177(86)90453-9.

Goldberg, M. D., D. S. Crosby, and L. Zhou (2001), The limb adjustment of AMSU-A observations: Methodology and validation, *J. Appl. Meteorol.*, *40*, 70–83, doi:10.1175/1520-0450(2001)040<0070:TLAOAA>2.0.CO;2.

Hauchecorne, A., and M.-L. Chanin (1980), Density and temperature profiles obtained by lidar between 35 and 70 km, *Geophys. Res. Lett.*, *7*, 565–568, doi:10.1029/GL007i008p00565.

Hauchecorne, A., and M.-L. Chanin (1983), Mid-latitude Lidar observations of planetary waves in the middle atmosphere during the winter of 1981–1982, *J. Geophys. Res.*, *88*, 3843–3849, doi:10.1029/JC088iC06p03843.

Hauchecorne, A., M. L. Chanin, and P. Keckhut (1991), Climatology and trends of the middle atmospheric temperature (33–87 km) as seen by Rayleigh lidar above south of France, *J. Geophys. Res.*, *96*, 15,297–15,309, doi:10.1029/91JD01213.

Ho, S.-P., Y.-H. Kuo, Z. Zeng, and T. C. Peterson (2007), A comparison of lower stratosphere temperature from microwave measurements with CHAMP GPS RO data, *Geophys. Res. Lett.*, *34*, L15701, doi:10.1029/2007GL030202.

Karbou, F., F. Aires, C. Prigent, and L. Eymard (2005), Potential of Advanced Microwave Sounding Unit-A (AMSU-A) and AMSU-B measurements for atmospheric temperature and humidity profiling over land, *J. Geophys. Res.*, *110*, D07109, doi:10.1029/2004JD005318.

Keckhut, P., A. Hauchecorne, and M.-L. Chanin (1993), A critical review of the data base acquired for the long-term surveillance of the middle atmosphere by the French Rayleigh lidars, *J. Atmos. Oceanic Technol.*, *10*, 850–867, doi:10.1175/1520-0426(1993)010<0850:ACROTD>2.0.CO;2.

Keckhut, P., J. D. Wild, M. Gelman, A. J. Miller, and A. Hauchecorne (2001), Investigations on long-term temperature changes in the upper stratosphere using lidar data and NCEP analyses, *J. Geophys. Res.*, *106*, 7937–7944, doi:10.1029/2000JD900845.

Keckhut, P., et al. (2004), Review of ozone and temperature lidar validations performed within the framework of the Network for the Detection of Stratospheric Change, *J. Environ. Monit.*, *6*, 721–733, doi:10.1039/b404256e.

Keckhut, P., et al. (2011), An evaluation of uncertainties in monitoring middle atmosphere temperatures with the ground-based lidar network in support of space observations, *J. Atmos. Sol. Terr. Phys.*, *73*, 627–642, doi:10.1016/j.jastp.2011.01.003.

Kurylo, M. J., and S. Solomon (1990), *Network for the Detection of Stratospheric Change: A Status and Implementation Report*, NASA, Washington, D. C.

Liu, Y., C. X. Liu, H. P. Wang, X. Tie, S. T. Gao, D. Kinnison, and G. Brasseur (2008), Atmospheric tracers during the 2003–2004 stratospheric warming event and impact of ozone intrusions in the troposphere, *Atmos. Chem. Phys. Discuss.*, *8*, 13,633–13,666, doi:10.5194/acpd-8-13633-2008.

Manney, G. L., K. Krüger, J. L. Sabutis, S. A. Sena, and S. Pawson (2005), The remarkable 2003–2004 winter and other recent warm winters in the Arctic stratosphere since the late 1990s, *J. Geophys. Res.*, *110*, D04107, doi:10.1029/2004JD005367.

Manney, G. L., et al. (2008), The evolution of the stratopause during the 2006 major warming: Satellite data and assimilated meteorological analyses, *J. Geophys. Res.*, *113*, D11115, doi:10.1029/2007JD009097.

Mo, T. (2009), A study of the NOAA-15 AMSU-A brightness temperatures from 1998 through 2007, *J. Geophys. Res.*, *114*, D11110, doi:10.1029/2008JD011267.

Mo, T. (2010), Postlaunch calibration of the NOAA-19 Advanced Microwave Sounding Unit-A, *J. Geophys. Res.*, *115*, D08111, doi:10.1029/2009JD013177.

Nash, J., and G. F. Forrester (1986), Long-term monitoring of stratospheric temperature trends using radiance measurements obtained by the TIROS-N series of NOAA spacecraft, *Adv. Space Res.*, *6*, 37–44, doi:10.1016/0273-1177(86)90455-2.

Ramaswamy, V., et al. (2001), Stratospheric temperature trends observations and model simulations, *Rev. Geophys.*, *39*, 71–122, doi:10.1029/1999RG000065.

Randel, W. J., et al. (2004), The SPARC intercomparison of middle-atmosphere climatologies, *J. Clim.*, *17*, 986–1003, doi:10.1175/1520-0442(2004)017<0986:TSIOMC>2.0.CO;2.

Randel, W. J., et al. (2009), An update of observed stratospheric temperature trends, *J. Geophys. Res.*, *114*, D02107, doi:10.1029/2008JD010421.

Shine, K. P., et al. (2003), A comparison of model simulated trend in stratospheric temperature, *Q. J. R. Meteorol. Soc.*, *129*, 1565–1588, doi:10.1256/qj.02.186.

Shine, K. P., J. J. Barnett, and W. J. Randel (2008), Temperature trends derived from Stratospheric Sounding Unit radiances: The effect of increasing CO_2 on the weighting function, *Geophys. Res. Lett.*, *35*, L02710, doi:10.1029/2007GL032218.

Steinbrecht, W., et al. (2006), Long-term evolution of upper stratospheric ozone at selected stations of the Network for the Detection of Stratospheric Change (NDSC), *J. Geophys. Res.*, *111*, D10308, doi:10.1029/2005JD006454.

Steinbrecht, W., T. J. McGee, L. W. Twigg, H. Claude, F. Schönenborn, G. K. Sumnicht, and D. Silbert (2009a), Intercomparison of stratospheric ozone and temperature profiles during the October 2005 Hohenpeissenberg Ozone Profiling Experiment (HOPE), *Atmos. Meas. Tech.*, *2*, 125–145, doi:10.5194/amt-2-125-2009.

Steinbrecht, W., et al. (2009b), Ozone and temperature trends in the upper stratosphere at five stations of the Network for the Detection of Atmospheric Composition Change, *Int. J. Remote Sens.*, *30*, 3875–3886, doi:10.1080/01431160902821841.

Steiner, A. K., G. Kirchengast, M. Borsche, U. Foelsche, and T. Schoengassner (2007), A multi-year comparison of lower stratospheric temperatures from CHAMP radio occultation data with MSU/AMSU records, *J. Geophys. Res.*, *112*, D22110, doi:10.1029/2006JD008283.

Wilson, R., M. L. Chanin, and A. Hauchecorne (1991), Gravity waves in the middle atmosphere observed by Rayleigh lidar 2. Climatology, *J. Geophys. Res.*, *96*, 5169–5183, doi:10.1029/90JD02610.

Wu, D. L. (2004), Mesoscale gravity wave variances from AMSU-A radiances, *Geophys. Res. Lett.*, *31*, L12114, doi:10.1029/2004GL019562.

C. Claud, Laboratoire de Meteorologie Dynamique IPSL/UMR 8539, Ecole Polytechnique, F-91128 Palaiseau, France.

B. M. Funatsu, A. Hauchecorne, and P. Keckhut, Laboratoire Atmosphères, Milieux, Observations Spatiales, IPSL/UMR 8190, Université Versailles-Saint Quentin, F-78280 Guyancourt, France. (funatsu@latmos.ipsl.fr)

W. Steinbrecht, Meteorologisches Observatorium, Hohenpeissenberg, D-82383, Germany.